Journal of Sound and Vibration 479 (2020) 115400

Contents lists available at ScienceDirect

Journal of Sound and Vibration

journal homepage: www.elsevier.com/locate/jsvi

Active acoustic cloaking of cylindrical shells in low Mach number flow

Briscoe Kerferd [a], Daniel Eggler [a,*], Mahmoud Karimi [b], Nicole Kessissoglou [a]

[a] School of Mechanical and Manufacturing Engineering, The University of New South Wales, Sydney, 2052, Australia
[b] Centre for Audio, Acoustics and Vibration, University of Technology Sydney, Sydney, Australia

ARTICLE INFO

Article history:
Received 9 December 2019
Received in revised form 5 April 2020
Accepted 17 April 2020
Available online 21 April 2020
Handling Editor: A Tsouvalas

Keywords:
Cloaking
Active control
Mean flow
Vibro-acoustics
Cylindrical shell

ABSTRACT

The vibro-acoustic response of a two-dimensional cylindrical shell in low Mach number flow is herein derived. The analytical model takes into account the structural elasticity and coupling of the shell vibration with its interior and exterior acoustic fields in the presence of a moving fluid. The cylindrical shell is modelled using Donnell-Mushtari theory. Taylor transformations are employed to transfer the convected wave equation into the ordinary wave equation which was then solved using scattering theory. Three excitation cases corresponding to a plane wave, an external monopole source and a radial point force applied directly to the shell are considered. Shell circumferential resonances and interior acoustic resonances are identified. Two active control strategies are then applied to acoustically cloak the cylindrical shell at its acoustic and structural resonances. The first control approach employs acoustic control sources in the exterior fluid domain. In the second approach, control forces are applied to directly excite the elastic shell, whereby the structural response is actively modified to manipulate the scattered and radiated acoustic fields arising from plane wave excitation of the shell. Results show that the second approach is superior in terms of both reduced control effort and cloaking of the global exterior domain. For both control approaches, the performance of the active cloak is shown to deteriorate if the convected flow field is not accounted for in the control process.

1. Introduction

Acoustic cloaking has received significant interest in recent years with potential applications for stealth, masking, and reduction of anthropogenic noise. Passive cloaking approaches are well established, namely using a coordinate transformation approach wherein acoustic metamaterials are designed to render a region acoustically invisible. Metamaterial cloaks have been designed with functionally graded density, commonly referred to as inertial cloaks [1], or by jointly varying the metamaterial stiffness and density to guide the acoustic field around a cloaked region [2]. Multilayered cloaks using isotropic and metamaterial layers have also been proposed [3,4]. Popa et al. [5,6] applied the coordinate transformation method for the design of an acoustic ground cloak. Alternative passive methods using impedance matching skins with subwavelength inclusions, or through scattering cancellation using a specially designed isotropic elastic layer, have been explored [7,8]. Various active cloaking techniques have been proposed that can be broadly categorised as either exterior

* Corresponding author.
E-mail address: d.eggler@unsw.edu.au (D. Eggler).

https://doi.org/10.1016/j.jsv.2020.115400

cloaking or interior cloaking. Exterior cloaking, in which control sources are located outside of the cloaked region, was achieved using multipole sources to cloak a body from an incident field [9–12]. Interior cloaking, in which control sources are located within the cloaked region, has been demonstrated using piezoelectric coatings [13–16], or a discrete number of secondary sources to cancel the scattered field [17–20].

The aforementioned studies on the design of passive cloaks ignore the Doppler effect associated with convected flow of the surrounding acoustic medium. For stealth purposes in aeronautical and maritime applications, cloaking of a body in a moving fluid is required. Cloaking in mean flow was first demonstrated with a passive acoustic ground cloak in a moving fluid medium, which was theoretically constructed using a space-time transformation method [21]. Ryoo and Jeon [22] expanded on the work by Huang et al. [23], taking into account the effects of fluid compressibility and flow non-uniformity. Iemma and Palma [24] presented a convective correction for metamaterial cloaks originally designed for a stationary acoustic medium, which was found to effectively cloak a 2D cylinder from monopole excitation in both stationary and low Mach number flow. An increasing Mach number yielded diminished cloaking performance attributed to the low Mach number formulation of the governing equations in the cloak design. Huang et al. [25] proposed an optimisation routine to cancel turbulent noise from high Reynolds number flow over a cylinder by varying the metamaterial properties of the cloak using the method of steepest descent. More recently, they designed an acoustic cloak for an aerofoil in turbulent flow that was insensitive to frequency variations [26]. As an alternative to passive cloaking in mean flow, acoustic cloaking of a 2D rigid cylinder in low Mach number flow using an active control approach was recently proposed [27]. Failure to account for potential flow was shown to result in adverse constructive interference that enhanced the original acoustic field.

The current paper extends the recent study by Eggler et al. [27] on acoustic cloaking of a rigid cylinder, to consider an elastic cylindrical shell in low Mach number flow. A number of studies have investigated the vibrational responses of an elastic structure in convected flow, although to the best of the authors' knowledge, there is very little literature on the acoustic responses of an elastic structure in a moving fluid. Dynamic responses have been analytically studied for a cylindrical shell in cross flow [28] and axial flow [29]. Amabili and Garziera [30] reported a decrease in the eigenfrequencies of a cylindrical shell in axial flow with increasing flow speed. Taylor [31] pioneered a transformation method to derive the acoustic field arising from a vibrating surface in low Mach number potential flow. The method was then employed to model acoustic generation by pulsating and vibrating elastic spheres in homentropic potential flow.

In this work, active acoustic cloaking of an elastic cylindrical shell in convected flow is presented. The active control methodology depends on prediction of the vibro-acoustic responses of the elastic shell arising from excitation due to the primary incident field and the control sources. To this end, we utilise Taylor's transformation method to derive the structural and acoustic responses of an elastic cylindrical shell excited by acoustic sources or localised mechanical forces in a moving fluid. The cylindrical shell is modelled using standard shell theory, in which the shell displacements are coupled with the interior and exterior acoustic fields. Taylor transformations are then applied to the interior and exterior acoustic fields to reduce the convected wave equation to the standard Helmholtz equation, which is subsequently solved using scattering theory for an elastic shell. The vibro-acoustic responses of the cylindrical shell with and without the presence of flow are compared. Two active control approaches are then employed to acoustically cloak the shell at its structural and acoustic resonances. The first control approach called active noise cloaking employs acoustic control sources in the exterior fluid domain uniformly distributed around the cylindrical shell. In the second approach, termed active structural acoustic cloaking, control forces are applied to directly excite the elastic shell. The structural response is actively modified to manipulate the scattered and radiated acoustic fields arising from plane wave excitation of the shell. The effectiveness of the two active control approaches are compared. Further, the performance of the acoustic cloaks with and without accounting for convective flow is evaluated.

2. Analytical formulation

2.1. Elastic cylindrical shell

A 2D elastic cylindrical shell is located in a flow of free stream velocity U_∞ as shown in Fig. 1. Donnell-Mushtari shell theory with a Flügge–Byrne–Lur'ye modifying operator to account for the midplane displacements and the curvature of the shell is employed. The equations of motion in the radial and tangential directions are respectively given by [32]

$$\frac{\partial v(\theta,t)}{\partial\theta}+\left(1+\frac{1}{\beta^2}\left(1+\frac{\partial^2}{\partial\theta^2}\right)^2\right)w(\theta,t)=-\frac{\rho(1-\nu^2)a^2}{E}\frac{\partial^2 w(\theta,t)}{\partial t^2}, \tag{1}$$

$$\frac{\partial^2 v(\theta,t)}{\partial\theta^2}+\frac{\partial w(\theta,t)}{\partial\theta}=\frac{\rho(1-\nu^2)a^2}{E}\frac{\partial^2 v(\theta,t)}{\partial t^2}, \tag{2}$$

where w and v are the radial and tangential shell displacements, respectively, a is the mid-thickness shell radius, $\beta=\sqrt{12}a/h$ is the non-dimensional shell thickness parameter, h is the shell thickness, and E, ν, ρ are respectively the Young's modulus, Poisson's ratio and density of the shell.

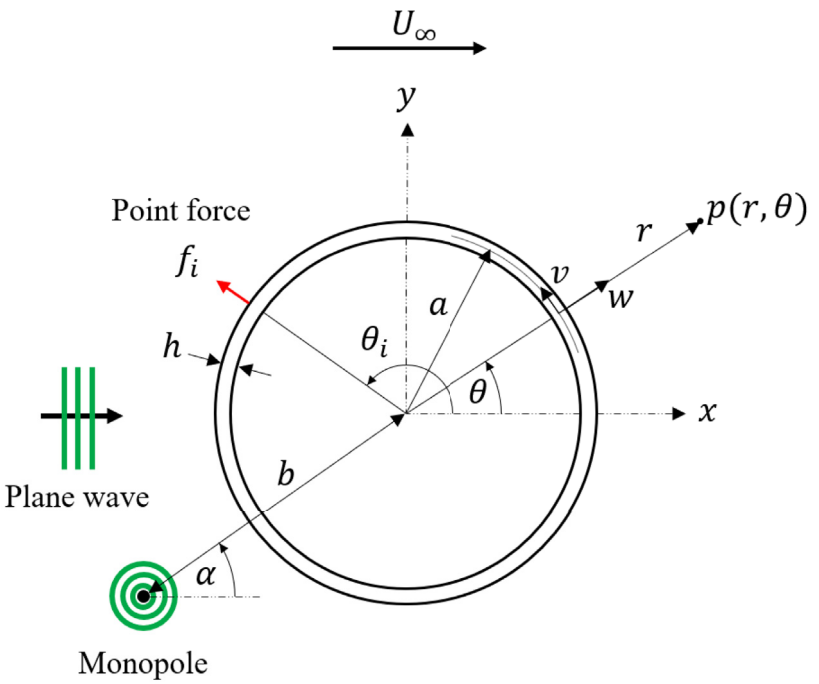

Fig. 1. Schematic diagram of the elastic cylindrical shell showing the geometric representation of the system, the direction of the free stream velocity, and excitation of the shell by acoustic sources and a localised point force.

The equation of motion for the shell radial displacement is modified to consider a localised point force as well as the acoustic pressure loading on the interior and exterior surfaces of the shell. Assuming time-harmonic separable solutions for w and v such that $w(\theta,t)=w(\theta)e^{-\mathrm{i}\omega t}$ and $v(\theta,t)=v(\theta)e^{-\mathrm{i}\omega t}$, where $\mathrm{i}=\sqrt{-1}$ and ω is the angular frequency, the equations of motion in the radial and tangential directions become [33]

$$\left(D\frac{d^4}{d\theta^4}+D\beta^2-\rho h\omega^2+D\left(1+2\frac{d^2}{d\theta^2}\right)\right)w(\theta)+D\beta^2\frac{d}{d\theta}v(\theta)=p_{\mathrm{int}}(a,\ \theta)-p_{\mathrm{ext}}(a,\theta)\ +f_i\delta(\theta-\theta_i), \tag{3}$$

$$G\frac{d^2}{d\theta^2}v(\theta)+G\frac{d}{d\theta}w(\theta)+\rho h\omega^2 v(\theta)=0. \tag{4}$$

$G=Eh/(a^2(1-\nu^2))$ and $D=G/\beta^2$ are shell stiffness parameters. $p_{\mathrm{int}}(r,\theta)$ is the interior acoustic pressure. The exterior acoustic pressure $p_{\mathrm{ext}}(r,\theta)$ comprises both the incident acoustic pressure due to an acoustic source, $p_{\mathrm{inc}}(r,\theta)$, and the combined scattered and radiated pressure arising from acoustic excitation of the shell, $p_{\mathrm{sc/rad}}(r,\theta)$. That is, for acoustic excitation, $p_{\mathrm{ext}}(r,\theta)=p_{\mathrm{inc}}(r,\theta)+p_{\mathrm{sc/rad}}(r,\theta)$. For structural excitation of the shell, the exterior acoustic pressure comprises only the structure-borne acoustic pressure, $p_{\mathrm{rad}}(r,\theta)$, such that $p_{\mathrm{ext}}(r,\theta)=p_{\mathrm{rad}}(r,\theta)$. f_i and θ_i denote the amplitude and angular location of the i^{th} localised point force, respectively, and $\delta(\theta-\theta_i)$ is the Dirac delta function. The shell radial and tangential displacements are expressed in terms of their Fourier coefficients, w_n and v_n, by summing over the modal order n as follows [32]

$$w(\theta)=\sum_{n=-\infty}^{\infty}w_n e^{\mathrm{i}n\theta}, \tag{5}$$

$$v(\theta)=\sum_{n=-\infty}^{\infty}v_n e^{\mathrm{i}n\theta}. \tag{6}$$

Three different excitation cases are herein considered corresponding to an incident plane wave travelling in the direction of the flow, a monopole source located in the exterior acoustic domain and a radial point force applied directly to the shell, as shown in Fig. 1. Assuming time harmonic excitation, the incident acoustic pressure fields in the absence of flow for plane wave and monopole source excitation are respectively given by [34]

$$p_{\text{inc}}(\mathbf{x},t)=\sum_{n=-\infty}^{\infty}a_n\frac{J_n(k_\text{a}r)}{J_n(k_\text{a}a)}e^{\text{i}n\theta}e^{-\text{i}\omega t}, \tag{7}$$

$$p_{\text{inc}}(\mathbf{x},t)=H_0(k_\text{a}R)e^{-\text{i}\omega t}, \tag{8}$$

where R is the distance from the monopole source to the field point $\mathbf{x}=(r,\theta)$, J_n is the Bessel function of the first kind of order n, H_0 is the zeroth order Hankel function of the first kind, $()'$ is the derivative with respect to the argument and k_a is the acoustic wavenumber. The incident field coefficient for a plane wave is $a_n=\text{i}^nJ_n'(k_\text{a}a)$ [34]. Equations (7) and (8) must be modified to account for convection effects as outlined in Sections 2.3 and 2.4, respectively.

2.2. Transformation of the exterior and interior acoustic potential

The exterior and interior acoustic fields are evaluated in terms of the acoustic potential $\varphi_\text{a}(\mathbf{x},t)$ using the linearised potential flow formulation of the convected wave equation which is given by [35–38]

$$\left(\frac{\partial}{\partial t}+\nabla\varphi_\text{v}\cdot\nabla\right)^2\varphi_\text{a}-c_f^2\nabla^2\varphi_\text{a}=0, \tag{9}$$

where $\varphi_\text{v}(\mathbf{x})$ is the velocity potential governing the mean flow of the convected field. This equation is valid for isentropic, inviscid and irrotational flow and neglects terms of $\text{O}(M^2)$ where $M=U_\infty/c_f$ is the Mach number and c_f is the speed of sound in the fluid. As such, our analysis is limited to low Mach number potential flow ($M^2\ll1$). Since the physical system has two distinct acoustic fields, Eq. (9) must be solved separately for both the exterior acoustic potential $\varphi_{\text{a,ext}}(\mathbf{x},t)$ and the interior acoustic potential $\varphi_{\text{a,int}}(\mathbf{x},t)$. The reference spatial and temporal coordinates $(\mathbf{x},t)$ are mapped to the transformed coordinates $(\mathbf{X},T)$ according to the Taylor transformations given by [37]

$$\mathbf{X}=\mathbf{x},\quad T=t+\frac{\varphi_\text{v}}{c_f^2}. \tag{10}$$

Note, $\mathbf{x}=(r,\theta)$ and $\mathbf{X}=(\widehat{r},\widehat{\theta})$ respectively denote the coordinates in the original and transformed cylindrical coordinate systems for a given field point. Employing these transformations reduces Eq. (9) to the Helmholtz equation in the transformed coordinates, which can then be solved using standard scattering theory. However, the acoustic-structure interaction between the elastic structure and the convected acoustic field complicates the solution for the scattered and structurally radiated sound field. Taylor [31] proposed that the acoustic effects of a vibrating surface in potential flow defined by $\Gamma(\mathbf{x},t)=\overline{\Gamma}(\mathbf{x})+\sigma(\mathbf{x},t)=0$ could be captured using the following boundary condition

$$\left[\nabla\varphi_\text{a}\cdot\frac{\nabla\overline{\Gamma}}{|\nabla\overline{\Gamma}|}\right]_{\overline{\Gamma}=0}=\left[-\frac{1}{|\nabla\overline{\Gamma}|}\left(\frac{\partial}{\partial t}+\nabla\varphi_\text{v}\cdot\nabla\right)\sigma+\sigma\frac{\nabla\overline{\Gamma}}{|\nabla\overline{\Gamma}|^3}\cdot\nabla(\nabla\varphi_\text{v}\cdot\nabla\overline{\Gamma})\right]_{\overline{\Gamma}=0}, \tag{11}$$

where $\overline{\Gamma}(\mathbf{x})=0$ defines the mean position of the surface and $\sigma(\mathbf{x},t)$ is the time-varying component of the surface position. To simplify this boundary condition, we define $\overline{\Gamma}$ and σ by restricting our analysis to an elastic cylindrical shell in plane strain, which results in $\overline{\Gamma}=r-a$ and $\sigma(\theta,t)=-w(\theta)e^{-\text{i}\omega t}$. The velocity potential for a 2D cylinder in cylindrical coordinates is defined by [39]

$$\varphi_\text{v}(\mathbf{x})=U_\infty\left(r+\frac{a^2}{r}\right)\cos\theta. \tag{12}$$

For the case of a finite cylindrical shell in potential flow, a numerical solution to the Laplace equation for the velocity potential would be required. Substituting the expressions for $\overline{\Gamma}$, σ and φ_v into the boundary condition given by Eq. (11) and simplifying the resulting expression yields the boundary condition for the exterior acoustic potential as

$$\left[\frac{\partial}{\partial r}\varphi_{\text{a,ext}}\right]_{r=a}=-\sum_{n=-\infty}^{\infty}\left(\text{i}\omega+\frac{2U_\infty}{a}(\cos\theta+\text{i}n\sin\theta)\right)w_ne^{\text{i}n\theta}e^{-\text{i}\omega t}. \tag{13}$$

Recognising that the interior acoustic domain is stationary (i.e. $U_\infty=0$), the boundary condition for the interior acoustic potential is given by

$$\left[\frac{\partial}{\partial r}\varphi_{\mathrm{a,int}}\right]_{r=a} = -\sum_{n=-\infty}^{\infty} \mathrm{i}\omega w_n e^{\mathrm{i}n\theta} e^{-\mathrm{i}\omega t}. \tag{14}$$

The solution to the equations of motion given by Eqs. (3) and (4) is herein derived for the case of plane wave excitation. $\varphi_{\mathrm{a,ext}}(\mathbf{x},t)$ and $\varphi_{\mathrm{a,int}}(\mathbf{x},t)$ are first expressed as their transformed equivalents, denoted by $\widehat{\varphi}_{\mathrm{a,ext}}(\mathbf{X},T)$ and $\widehat{\varphi}_{\mathrm{a,int}}(\mathbf{X},T)$, respectively. As Eq. (9) reduces to the Helmholtz equation under the Taylor transformations, $\widehat{\varphi}_{\mathrm{a,ext}}$ and $\widehat{\varphi}_{\mathrm{a,int}}$ are solutions to the exterior and interior Helmholtz equations respectively, and can be expressed in their general forms as follows

$$\widehat{\varphi}_{\mathrm{a,ext}} = \sum_{n=-\infty}^{\infty} \left(\widehat{a}_n \frac{J_n(k_{\mathrm{a}}\widehat{r})}{J_n'(k_{\mathrm{a}}a)} + \widehat{b}_n \frac{H_n(k_{\mathrm{a}}\widehat{r})}{H_n'(k_{\mathrm{a}}a)}\right) e^{\mathrm{i}n\widehat{\theta}} e^{-\mathrm{i}\omega T}, \tag{15}$$

$$\widehat{\varphi}_{\mathrm{a,int}} = \sum_{n=-\infty}^{\infty} \widehat{c}_n \frac{J_n(k_{\mathrm{a}}\widehat{r})}{J_n'(k_{\mathrm{a}}a)} e^{\mathrm{i}n\widehat{\theta}} e^{-\mathrm{i}\omega T}. \tag{16}$$

The first term on the right hand side of Eq. (15) corresponds to the transformed incident acoustic potential $\widehat{\varphi}_{\mathrm{a,inc}}(\mathbf{X},T)$ and the second term corresponds to the transformed scattered and radiated acoustic potential $\widehat{\varphi}_{\mathrm{a,sc/rad}}(\mathbf{X},T)$, where H_n is the Hankel function of the first kind of order n. $\widehat{a}_n$ denotes the coefficients describing the transformed incident acoustic potential, $\widehat{b}_n$ represents the coefficients for the transformed scattered/radiated acoustic potential, and $\widehat{c}_n$ are the coefficients for the transformed interior acoustic potential.

The boundary conditions in the transformed domain are obtained by applying Taylor's transformations to Eqs. (13) and (14) and substituting the expressions for the transformed acoustic potentials given by Eqs. (15) and (16), respectively. A system of algebraic equations for the unknown coefficients can be obtained by considering orthogonality of the Fourier series basis $e^{\mathrm{i}n\widehat{\theta}}$. First considering the exterior acoustic potential, applying Taylor's transformations to Eq. (13), substituting Eq. (15) for the transformed exterior acoustic potential, multiplying by $e^{-\mathrm{i}m\widehat{\theta}}$ and then integrating between 0 and 2π, results in an infinite set of integrals without a closed form solution. The infinite set of integrals can be represented by the matrix expression $\widehat{\mathbf{b}} = \mathbf{\Phi}\mathbf{w} - \widehat{\mathbf{a}}$, where $\widehat{\mathbf{a}}$ is a column vector containing the elements $\widehat{a}_n$, $\widehat{\mathbf{b}}$ is a column vector containing the elements $\widehat{b}_n$, and $\mathbf{w}$ is a column vector containing the shell radial Fourier coefficients w_n. $\mathbf{\Phi}$ is a matrix containing the elements Φ_{mn} given by the following expression

$$\Phi_{mn} = -\frac{1}{2\pi k_{\mathrm{a}}} \int_0^{2\pi} \left(\mathrm{i}\omega + \frac{2U_\infty}{a}(\cos\widehat{\theta} + \mathrm{i}n\sin\widehat{\theta})\right) e^{\mathrm{i}n\widehat{\theta}} e^{-\mathrm{i}m\widehat{\theta}} e^{\mathrm{i}\omega\varphi_{\mathrm{v}}/c_f^2} d\widehat{\theta}. \tag{17}$$

The elements Φ_{mn} are evaluated numerically via the trapezoidal method using $2n$ subintervals.

Now considering the interior acoustic potential, applying Taylor's transformations to Eq. (14) and substituting Eq. (16) yields the interior boundary condition in the transformed domain. Multiplying by $e^{-\mathrm{i}m\widehat{\theta}}$ and integrating between 0 and 2π results in $\widehat{c}_n = -\mathrm{i}c_f w_n$, thus directly relating the transformed interior acoustic potential to the shell radial displacement.

2.3. Solution for the exterior and interior acoustic pressure

The exterior and interior acoustic responses of the cylindrical shell in potential flow can now be solved using the shell equations of motion. The acoustic pressure is related to the acoustic potential using Bernoulli's equation as follows

$$p = -\rho_f \left(\frac{\partial}{\partial t}\varphi_{\mathrm{a}} + \nabla\varphi_{\mathrm{v}} \cdot \nabla\varphi_{\mathrm{a}}\right). \tag{18}$$

Taylor's transformations are applied to Eq. (18), neglecting terms of $\mathrm{O}(M^2)$, to relate the transformed exterior and interior acoustic pressures respectively denoted by $\widehat{p}_{\mathrm{ext}}(\mathbf{X},T)$ and $\widehat{p}_{\mathrm{int}}(\mathbf{X},T)$, to the corresponding transformed acoustic potentials given by Eqs. (15) and (16). The resulting expressions are evaluated at $\widehat{r} = a$ to yield

$$\widehat{p}_{\mathrm{ext}}(a,\ \widehat{\theta},\ T) = \rho_f \left(\sum_{n=-\infty}^{\infty} \left(\mathrm{i}\omega + \frac{2U_\infty}{a}\mathrm{i}n\sin\widehat{\theta}\right)\left(\widehat{a}_n \frac{J_n(k_{\mathrm{a}}a)}{J_n'(k_{\mathrm{a}}a)} + \widehat{b}_n \frac{H_n(k_{\mathrm{a}}a)}{H_n'(k_{\mathrm{a}}a)}\right) e^{\mathrm{i}n\widehat{\theta}}\right) e^{-\mathrm{i}\omega T}, \tag{19}$$

$$\widehat{p}_{\text{int}}(a,\ \widehat{\theta},T) = \mathrm{i}\omega\rho_f \sum_{n=-\infty}^{\infty} \widehat{c}_n \frac{J_n(k_\text{a}a)}{J_n'(k_\text{a}a)} e^{\mathrm{i}n\widehat{\theta}} e^{-\mathrm{i}\omega T}. \tag{20}$$

In the final step, Taylor's transformations are applied to Eqs. (3) and (4) to describe the shell's equations of motion in the transformed domain. Substituting Eqs. (19) and (20) into the transformed equations of motion and solving simultaneously with $\widehat{\mathbf{b}} = \mathbf{\Phi w} - \widehat{\mathbf{a}}$ and $\widehat{c}_n = -\mathrm{i}c_f w_n$ yields the following solution for the vector $\mathbf{w}$ of radial displacement coefficients

$$\mathbf{w} = (\mathbf{B} + \mathbf{D\Phi})^{-1}((\mathbf{D} - \mathbf{C})\widehat{\mathbf{a}}). \tag{21}$$

$\mathbf{B}$ is a diagonal matrix with elements given by

$$B_{nn} = D\left(1 - 2n^2 + n^4\right) + G\left(1 - \frac{Gn^2}{Gn^2 - \rho h\omega^2}\right) - \rho h\omega^2 - \rho_f \omega c_f \frac{J_n(k_\text{a}a)}{J_n'(k_\text{a}a)}, \tag{22}$$

and $\mathbf{C}$ and $\mathbf{D}$ are the matrices with elements given by

$$C_{mn} = \frac{\rho_f}{2\pi} \frac{J_n(k_\text{a}a)}{J_n'(k_\text{a}a)} \int_0^{2\pi} \left(\mathrm{i}\omega + \frac{2U_\infty}{a} \mathrm{i}n \sin\theta\right) e^{\mathrm{i}n\theta} e^{-\mathrm{i}m\theta} e^{-\mathrm{i}\omega\varphi_\text{v}/c_f^2} d\theta, \tag{23}$$

$$D_{mn} = \frac{\rho_f}{2\pi} \frac{H_n(k_\text{a}a)}{H_n'(k_\text{a}a)} \int_0^{2\pi} \left(\mathrm{i}\omega + \frac{2U_\infty}{a} \mathrm{i}n \sin\theta\right) e^{\mathrm{i}n\theta} e^{-\mathrm{i}m\theta} e^{-\mathrm{i}\omega\varphi_\text{v}/c_f^2} d\theta, \tag{24}$$

which are evaluated numerically via the trapezoidal method using $2n$ subintervals, as per Eq. (17).

The elements of $\widehat{\mathbf{a}}$ are defined by $\widehat{a}_n = a_n/\mathrm{i}\omega\rho_f$ such that $\widehat{\varphi}_{\text{a,inc}}$ describes an unconvected incident field when $\nabla\varphi_\text{v} = 0$, as per Eq. (18). The coefficients $\widehat{b}_n$ are evaluated using $\widehat{\mathbf{b}} = \mathbf{\Phi w} - \widehat{\mathbf{a}}$. The coefficients $\widehat{c}_n$ are evaluated using $\widehat{c}_n = -\ \mathrm{i}c_f w_n$. Finally, the exterior and interior acoustic pressures in the untransformed domain respectively denoted by p_{ext} and p_{int} can be expressed in terms of their resolved coefficients at a field point as follows

$$p_{\text{ext}}(\mathbf{x},\ t) = \rho_f \left(\tau(\mathbf{x}) + \sum_{n=-\infty}^{\infty} \zeta_n(\mathbf{x})\right) e^{-\mathrm{i}\omega t} e^{-\mathrm{i}\omega\varphi_\text{v}/c_f^2}, \tag{25}$$

$$\tau(\mathbf{x}) = k_\text{a}U_\infty \left(\frac{a^2}{r^2} - 1\right)\cos\theta \sum_{n=-\infty}^{\infty} \left(\left(\widehat{a}_n \frac{J_n'(k_\text{a}r)}{J_n'(k_\text{a}a)} + \widehat{b}_n \frac{H_n'(k_\text{a}r)}{H_n'(k_\text{a}a)}\right) e^{\mathrm{i}n\theta}\right), \tag{26}$$

$$\zeta_n(\mathbf{x}) = \left(\mathrm{i}\omega + \frac{U_\infty}{r}\left(1 + \frac{a^2}{r^2}\right)\mathrm{i}n \sin\theta\right)\left(\widehat{a}_n \frac{J_n(k_\text{a}r)}{J_n'(k_\text{a}a)} + \widehat{b}_n \frac{H_n(k_\text{a}r)}{H_n'(k_\text{a}a)}\right) e^{\mathrm{i}n\theta}, \tag{27}$$

$$p_{\text{int}}(\mathbf{x},t) = \mathrm{i}\omega\rho_f \sum_{n=-\infty}^{\infty} \widehat{c}_n \frac{J_n(k_\text{a}r)}{J_n'(k_\text{a}a)} e^{\mathrm{i}n\theta} e^{-\mathrm{i}\omega t}. \tag{28}$$

τ and ζ_n capture the effect of the radial and tangential components of potential flow on the acoustic pressure at any field point in the exterior domain, respectively.

2.4. Monopole and force excitation

For monopole source excitation, a modification to the solution process must be implemented. The transformed exterior acoustic potential given by Eq. (15) now becomes

$$\widehat{\varphi}_{\text{a,ext}} = \left(\frac{1}{\mathrm{i}\omega\rho_f} H_0(k_\text{a}\widehat{R}) + \sum_{n=-\infty}^{\infty} \left(\widehat{b}_n \frac{H_n(k_\text{a}\widehat{r})}{H_n'(k_\text{a}a)}\right) e^{\mathrm{i}n\widehat{\theta}}\right) e^{-\mathrm{i}\omega T}, \tag{29}$$

where $\widehat{R}$ is the distance between the monopole source and the field point $\mathbf{X} = (\widehat{r}, \widehat{\theta})$ in the transformed domain. Equation (19) is still used at the boundary, however, the incident field due to the monopole source must first be expressed in the cylinder's local coordinates. This is achieved with Graf's addition theorem [34], yielding

$$H_0(k_a\widehat{R}) = \sum_{n=-\infty}^{\infty} (-1)^n H_n(k_a b) J_n(k_a \widehat{r}) e^{in(\widehat{\theta}-\alpha)}. \tag{30}$$

Thus, for monopole source excitation $\widehat{a}_n = (1/i\omega\rho_f)(-1)^n H_n(k_a b) J_n'(k_a a) e^{-in\alpha}$. The procedure to find the coefficients $\widehat{b}_n$, $\widehat{c}_n$, and w_n remains the same as described previously. However, Eqs. (25)–(28) must be modified to account for phase changes associated with the effect of the fluid flow between the location of the monopole source and the field point [27,37]. For monopole excitation, the exterior and interior acoustic pressures in the untransformed domain are expressed as

$$p_{\text{ext}}(\mathbf{x}, t) = \rho_f \left(\tau(\mathbf{x}) + \zeta_{\text{inc}}(\mathbf{x}) + \left(\sum_{n=-\infty}^{\infty} \zeta_{n,\text{sc/rad}}(\mathbf{x}) \right) \right) e^{-i\omega t} e^{i\omega(\varphi_s - \varphi_v)/c_f^2}, \tag{31}$$

$$\tau(\mathbf{x}) = k_a U_\infty \left(\frac{a^2}{r^2} - 1 \right) \cos\theta \left(\frac{H_0'(k_a R)}{i\omega\rho_f} \frac{\partial R}{\partial r} + \sum_{n=-\infty}^{\infty} \widehat{b}_n \frac{H_n'(k_a r)}{H_n'(k_a a)} e^{in\theta} \right), \tag{32}$$

$$\zeta_{\text{inc}}(\mathbf{x}) = \left(i\omega + \frac{U_\infty}{r} \left(1 + \frac{a^2}{r^2} \right) \sin\theta \frac{\partial}{\partial\theta} \right) \left(\frac{1}{i\omega\rho_f} H_0(k_a R) \right), \tag{33}$$

$$\zeta_{n,\text{sc/rad}}(\mathbf{x}) = \left(i\omega + \frac{U_\infty}{r} \left(1 + \frac{a^2}{r^2} \right) in \sin\theta \right) \widehat{b}_n \frac{H_n(k_a r)}{H_n'(k_a a)} e^{in\theta}, \tag{34}$$

$$p_{\text{int}}(\mathbf{x}, t) = i\omega\rho_f \sum_{n=-\infty}^{\infty} \widehat{c}_n \frac{J_n(k_a r)}{J_n'(k_a a)} e^{in\theta} e^{-i\omega t} e^{i\omega\varphi_s/c_f^2}, \tag{35}$$

where τ now captures the effect of the radial component of potential flow on the external acoustic pressure due to monopole source excitation and ζ_{inc}, $\zeta_{n,\text{sc/rad}}$ respectively capture the effect of the tangential component of potential flow on the incident and scattered/radiated acoustic pressure. φ_s is the velocity potential evaluated at the monopole source location. The resultant acoustic pressure and shell displacement due to N monopole sources require the superposition of the individually evaluated results from each source such that

$$p_{\text{ext}}(r, \theta) = \sum_{j=1}^{N} p_{\text{ext},j}, \tag{36}$$

$$p_{\text{int}}(r, \theta) = \sum_{j=1}^{N} p_{\text{int},j}, \tag{37}$$

$$w(\theta) = \sum_{j=1}^{N} w_j(\theta). \tag{38}$$

When the cylindrical shell is directly excited by a radial point force, $p_{\text{ext}} = p_{\text{rad}}$ in Eq. (3) and the solution procedure follows that of plane wave excitation. In this case, the radial shell displacement is given by

$$\mathbf{w} = (\mathbf{B} + \mathbf{D}\boldsymbol{\Phi})^{-1}\mathbf{f}, \tag{39}$$

where the matrix elements for $\boldsymbol{\Phi}$, **B**, **D** are given by Eqs. (17), (22) and (24), respectively. $\mathbf{f}$ is a column vector containing the elements $f_n = f_i e^{-in\theta_i}/2\pi$. When N radial point forces are employed, the elements within the column vector for $\mathbf{f}$ become

$$f_n = \sum_{i=1}^{N} f_i \frac{e^{-in\theta_i}}{2\pi}. \tag{40}$$

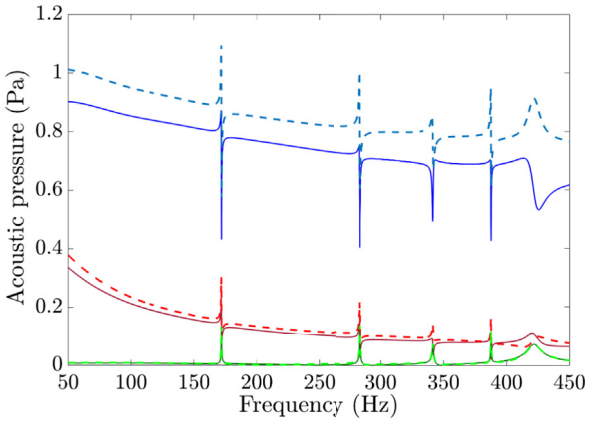

Fig. 2. Acoustic pressure (in Pascal) at $5a$ downstream of the cylindrical shell for plane wave excitation (blue lines), a monopole source located upstream at $(b, \alpha) = (2a, 0)$ (red lines), and a radial point force at $(\theta_i = \pi)$ (green lines) for $M = 0$ (dotted lines) and $M = 0.12$ (solid lines). (For interpretation of the references to colour in this figure legend, the reader is referred to the Web version of this article.)

3. Physical system results

An infinitely long elastic cylindrical shell of mean radius $a = 0.6$ m and thickness $h = 4$ mm was modelled, with material properties corresponding to polyvinyl chloride of density $\rho = 1300$ kg/m^3, Young's modulus $E = 2.9$ GPa and Poisson's ratio $\nu = 0.3$. The interior and exterior fluid media of the shell are air with density $\rho_f = 1.225$ kg/m^3 and speed of sound $c_f = 343$ m/s. A truncated modal order of $n = 120$ was selected. This modal number ensured converged results when compared with numerical results from a finite element simulation using the commercial software COMSOL Multiphysics. Fig. 2 presents the acoustic pressure as a function of frequency at $(r, \theta) = (5a, 0)$ for three excitation cases corresponding to a plane wave, a monopole source located upstream at $(b, \alpha) = (2a, 0)$, and a point force at $\theta_i = \pi$. For each excitation case, results are presented in the absence of potential flow ($M = 0$) and in a convected flow field of Mach number $M = 0.12$. Fig. 2 shows that the effect of flow decreases the magnitude of the acoustic pressure for all excitation cases. Closer comparison of the relative change in magnitude under the effect of flow for each excitation case reveals a similar decrease in magnitude associated with each excitation type. For the frequency range considered in Fig. 2, the five resonances correspond to the first three acoustic spinning resonances, the first acoustic axisymmetric resonance, and the first structural resonance corresponding to the zeroth shell circumferential mode. Acoustic resonances were identified and categorised according to the interior field patterns described in Ref. [40]. Structural resonances were identified by the shell circumferential displacement pattern. The broad peak in Fig. 2 around 420 Hz corresponding to the first structural resonance is due to high radiation damping for the radially axisymmetric mode of the cylindrical shell [33,41].

Table 1 lists the frequencies for the first three acoustic spinning, acoustic axisymmetric and circumferential resonances of the cylindrical shell in the absence of potential flow ($M = 0$) and in convected flow ($M = 0.12$). The first three structural resonances correspond to the breathing (radially axisymmetric), bending and ovalling shell circumferential modes. The frequencies of the acoustic resonances are unaffected by the convected flow field. The presence of flow can yield a reduction in the resonance frequencies of the structural modes, as observed previously by Amabili and Garziera [30].

Fig. 3 presents contour plots of the acoustic pressure fields in the absence of potential flow (left column) and in the presence of a convected flow field of $M = 0.12$ (right column) for the first acoustic spinning resonance of the cylindrical shell due to excitation by an incident plane wave (Fig. 3(a)), a monopole source located at $(b, \alpha) = (2a, 0)$ (Fig. 3(b)), and a radial

Table 1
Resonance frequencies (in Hz) for the first three acoustic spinning resonances, acoustic axisymmetric resonances and shell circumferential resonances of the cylindrical shell in the absence of flow ($M = 0$) and in the presence of convected flow ($M = 0.12$).

Flow case		$M = 0$	$M = 0.12$
Acoustic spinning resonances (Hz)	First	171.85	171.85
	Second	283.42	283.42
	Third	387.63	387.63
Acoustic axisymmetric resonances (Hz)	First	341.52	341.52
	Second	641.44	641.44
	Third	927.20	927.20
Shell circumferential resonances (Hz)	Breathing	420.97	420.85
	Bending	589.90	589.65
	Ovalling	933.36	933.36

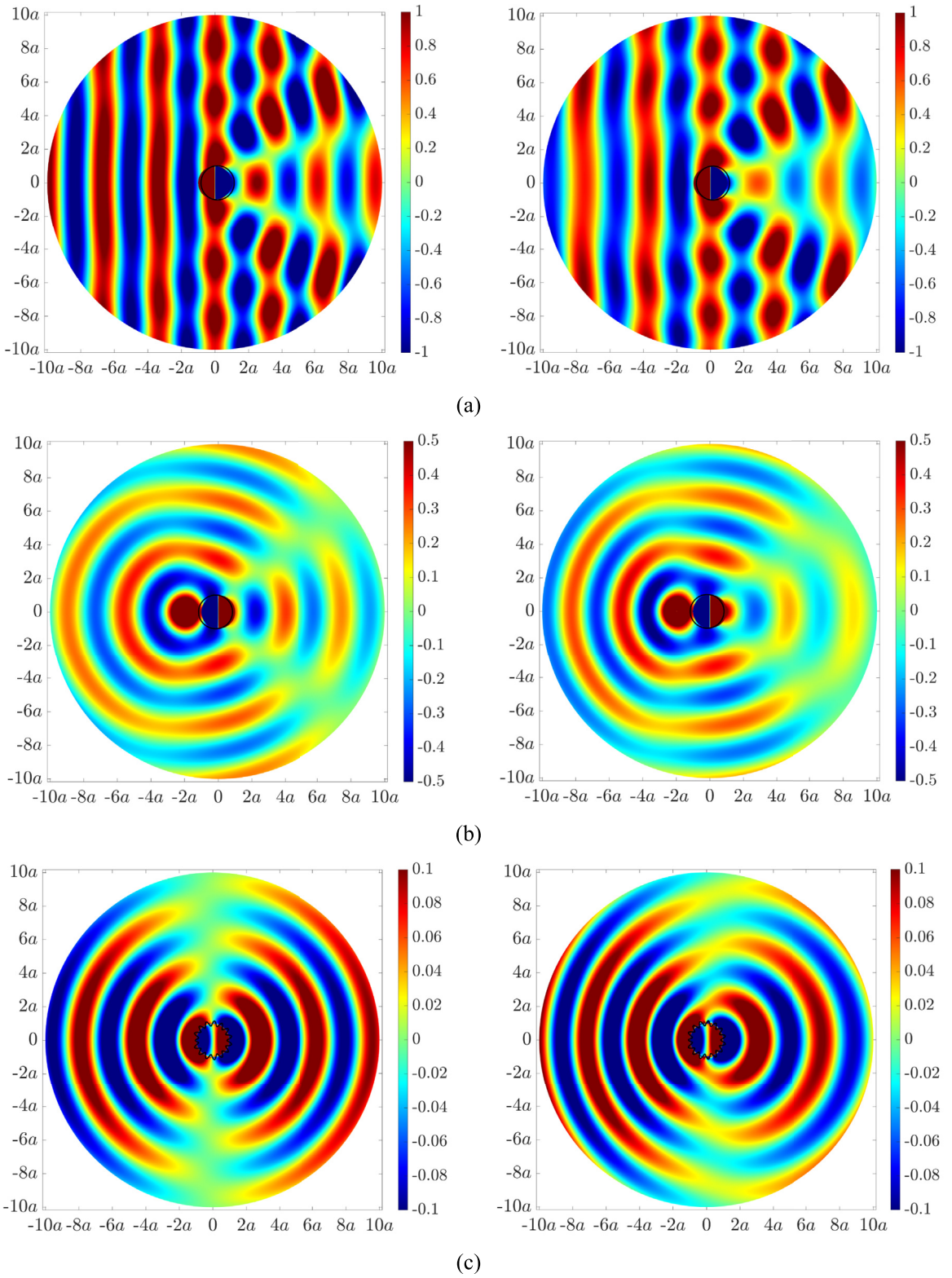

Fig. 3. Acoustic pressure (in Pascal) in a convected flow field of $M = 0$ (left) and $M = 0.12$ (right) at the first acoustic spinning resonance of the cylindrical shell due to excitation by (a) an incident plane wave, (b) a monopole source located at $(b, \alpha) = (2a, 0)$, and (c) a radial point force at $\theta_i = \pi$.

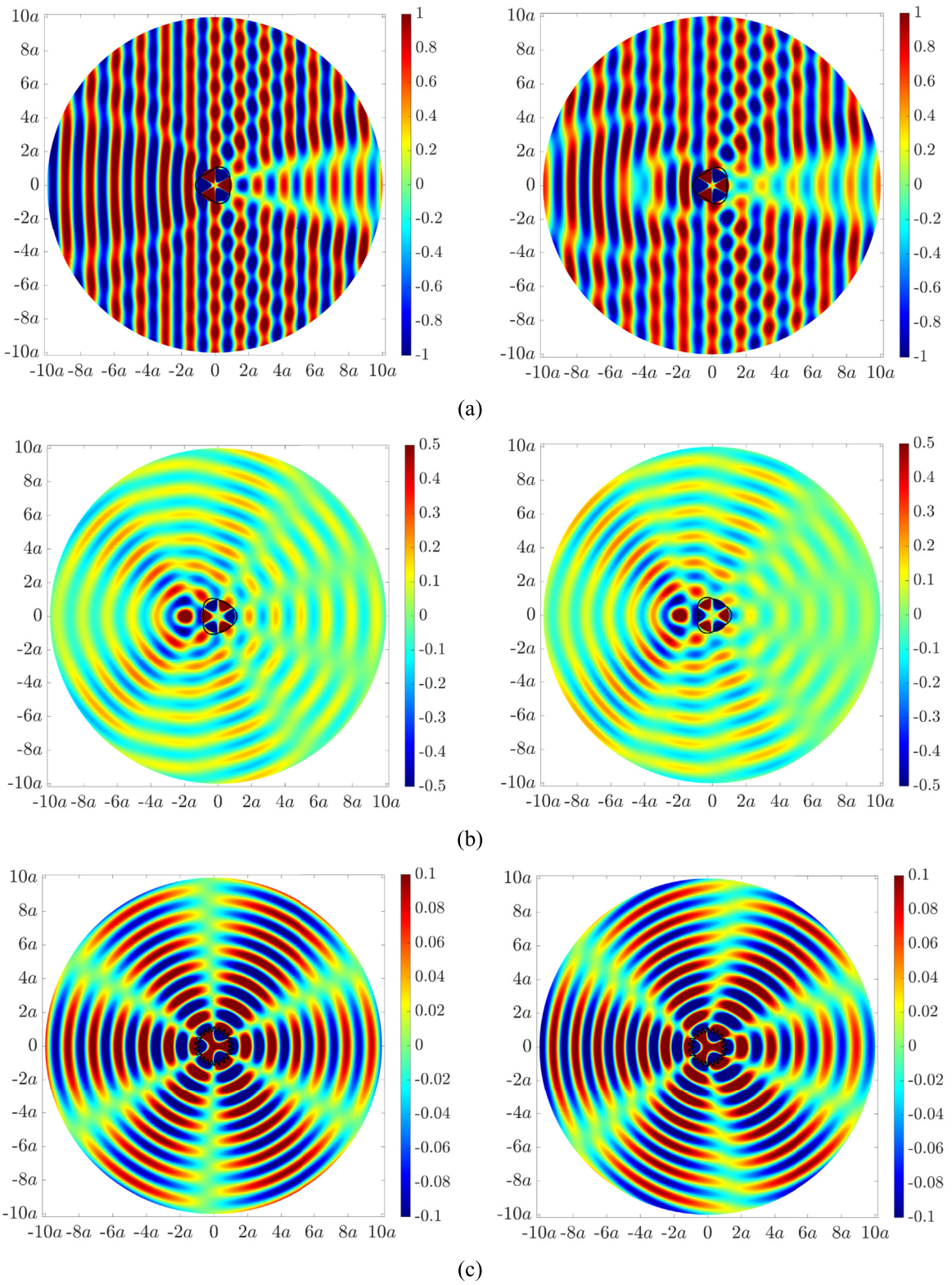

Fig. 4. Acoustic pressure (in Pascal) in a convected flow field of $M = 0$ (left) and $M = 0.12$ (right) at the third acoustic spinning resonance of the cylindrical shell due to excitation by (a) an incident plane wave, (b) a monopole source located at $(b, \alpha) = (2a, 0)$, and (c) a radial point force at $\theta_i = \pi$.

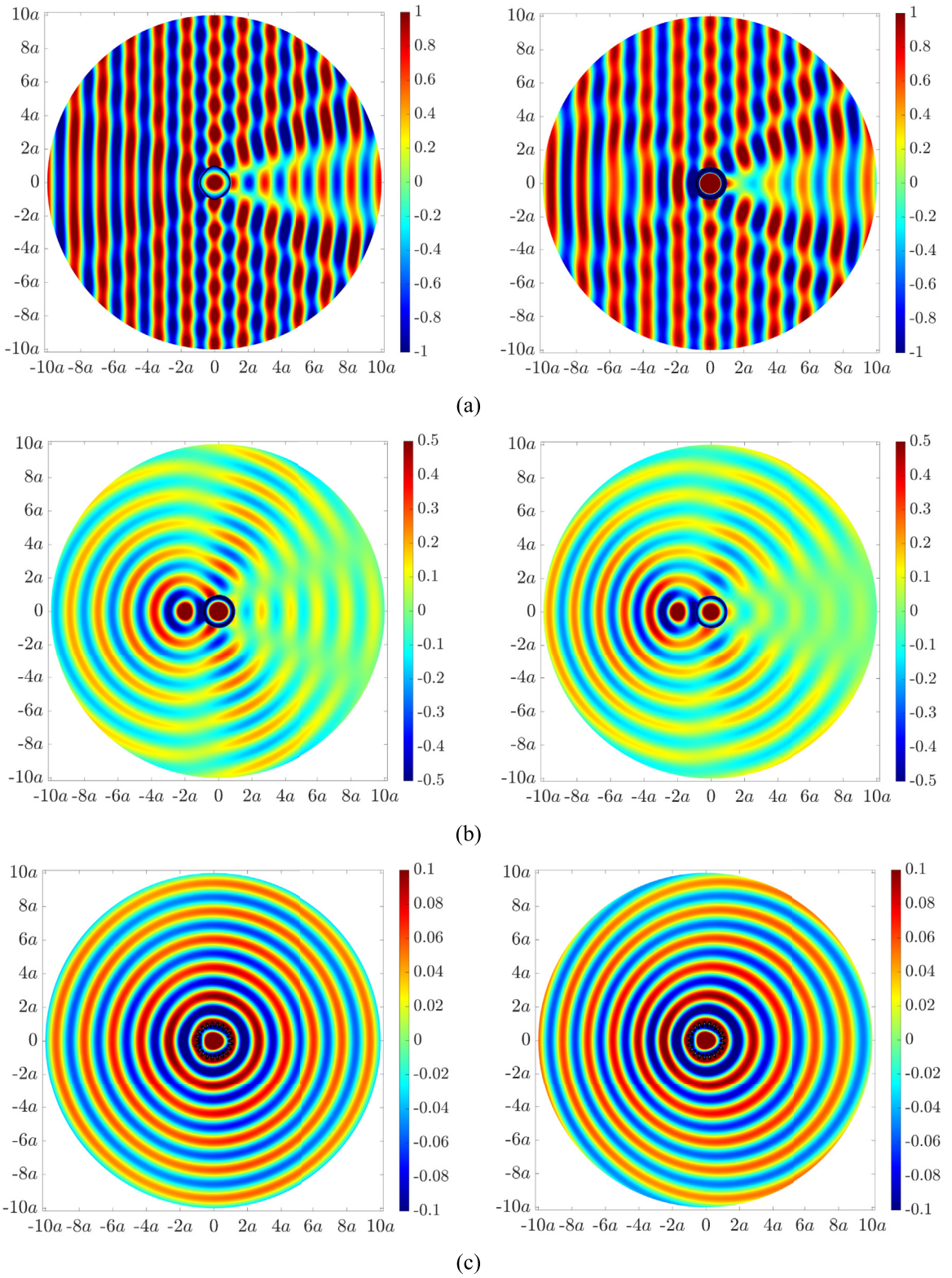

Fig. 5. Acoustic pressure (in Pascal) in a convected flow field of $M = 0$ (left) and $M = 0.12$ (right) at the first acoustic axisymmetric resonance of the cylindrical shell due to excitation by (a) an incident plane wave, (b) a monopole source located at $(b, \alpha) = (2a, 0)$, and (c) a radial point force at $\theta_i = \pi$.

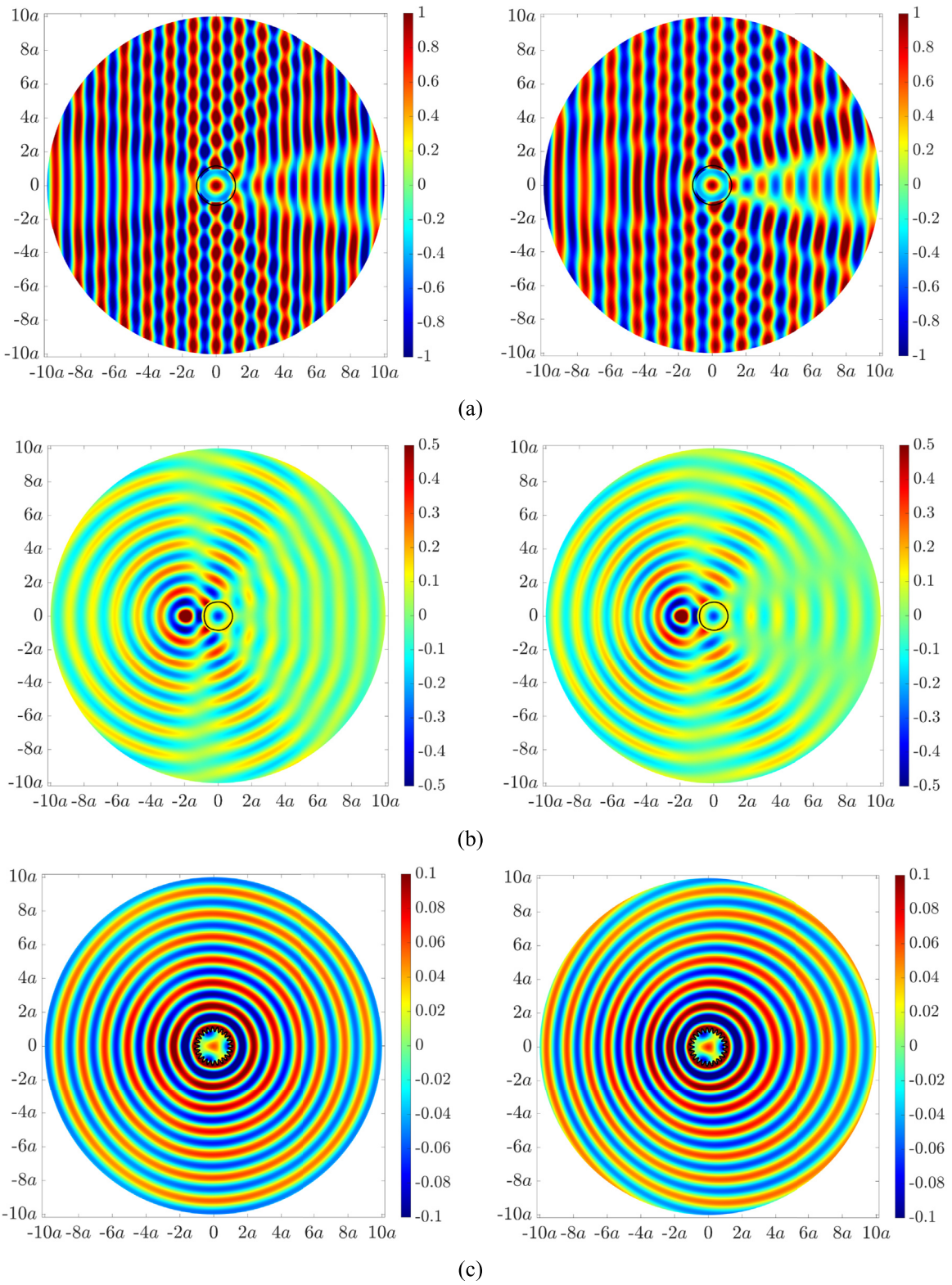

Fig. 6. Acoustic pressure (in Pascal) in a convected flow field of $M = 0$ (left) and $M = 0.12$ (right) at the first structural resonance of the cylindrical shell due to excitation by (a) an incident plane wave, (b) a monopole source located at $(b, \alpha) = (2a, 0)$, and (c) a radial point force at $\theta_i = \pi$.

point force at $\theta_i = \pi$ (Fig. 3(c)). Scattering both upstream and downstream of the shell is amplified by the presence of flow due to the Doppler effect, whereby expansion and contraction of the acoustic wavelength distorting the response can be observed. Fig. 4 shows similar results to that of Fig. 3, in which contour plots of the acoustic pressure for the third acoustic spinning resonance due to each excitation case, in the absence of potential flow (left column) and at $M = 0.12$ (right column), are shown. Enhanced scattering of the exterior acoustic field both upstream and downstream of the cylinder can be observed with increasing frequency. Similar contour plots of the acoustic pressure due to each excitation case are presented in Figs. 5 and 6 for the first acoustic axisymmetric resonance and first structural resonance, in the absence of potential flow (left column) and at $M = 0.12$ (right column). For a cylindrical shell of finite length, the presence of axial modes would result in a significantly higher number of structural resonances. Diffraction around the finite cylinder edges would yield greater scattering effects.

4. Cloaking methodology

We apply two active control strategies, namely active noise cloaking (ANCL) that utilises acoustic control sources and active structural acoustic cloaking (ASACL) that employs structural forces to actively modify the radiated sound field [18]. For ANCL, N monopole control sources and L microphone error sensors were equispaced in circumferential arrays around the cylinder at radial distances of $2a$ and $3a$, respectively. For ASACL, N point forces were applied to directly excite the shell, also uniformly distributed around the shell.

The cloaking algorithm is set up to minimise the acoustic field given by $\mathbf{e} = \mathbf{p}_{\mathrm{sc/rad}} + \mathbf{Zq}$, where $\mathbf{p}_{\mathrm{sc/rad}}$ corresponds to the combined scattered and radiated exterior acoustic pressure at the error sensor locations arising from excitation of the cylindrical shell by an incident plane wave, and $\mathbf{Zq}$ denotes the acoustic field generated by the control sources. $\mathbf{Z}$ is a matrix of acoustic transfer functions at the error sensor locations arising from each of the control sources, and $\mathbf{q}$ is a vector of control source amplitudes to be optimised. The optimisation process consists of minimising a quadratic cost function given by $J = \mathbf{e}^{\mathrm{H}}\mathbf{e}$ based on a feedforward adaptive least-mean-square algorithm [42]. The resultant optimal control source amplitudes are evaluated by solving $\partial J/\partial \mathbf{q} = 0$ and are obtained as

$$\mathbf{q} = -\left[\mathbf{Z}^{\mathrm{H}}\mathbf{Z}\right]^{-1}\mathbf{Z}^{\mathrm{H}}\mathbf{p}_{\mathrm{sc/rad}}, \tag{41}$$

where H denotes the Hermitian transpose. The current active control strategy requires *a priori* knowledge of the incident field as well the ability to directly measure the scattered and radiated acoustic pressure arising from the incident plane wave. There currently exist limited strategies to identify the scattered and radiated acoustic field separately from an incident acoustic field, for example, see Ref. [19,20,43,44].

A procedure outlined previously was used to determine the number of control sources and error sensors such that a percentage error function given by [18]

$$\Delta = \frac{||\mathbf{p}_{\mathrm{inc}}| - |\mathbf{p}_{\mathrm{cl}}||}{|\mathbf{p}_{\mathrm{inc}}|} \times 100\% \tag{42}$$

gives a predefined percentage error of $\Delta < 1\%$. In Eq. (42), $\mathbf{p}_{\mathrm{inc}}$ is a vector of incident acoustic pressures at the error sensors and $\mathbf{p}_{\mathrm{cl}}$ denotes the cloaked acoustic pressure at the error sensors. Table 2 summarises the control configurations employed for ANCL and ASACL at the first and third acoustic and structural resonances of the cylindrical shell in a convected flow field of $M = 0.12$. For each control configuration, the number of error sensors is greater than the number of control sources, thus ensuring that the least-mean-squares problem is overdetermined and yielding a unique solution provided by Eq. (41). The required number of control sources and error sensors to maintain $\Delta < 1\%$ increases with increasing frequency due to the reduction in the acoustic wavelength, as discussed previously [18].

The first and third acoustic and structural resonances of the cylindrical shell under incident plane wave excitation in a convected flow field of $M = 0.12$ are herein examined for the cloaking process. Active acoustic cloaking using either ANCL (left column) or ASACL (right column) is presented in Fig. 7 for the first acoustic spinning resonance (Fig. 7(a)), the first acoustic

Table 2
Cloaked resonance frequencies with number of control sources (N) and error sensors (L) for ANCL and ASACL in a convected flow field of $M = 0.12$.

		Frequency (Hz)	ANCL		ASACL	
			N	L	N	L
Spinning resonances	First	171.85	14	29	9	14
	Third	387.63	20	41	14	22
Axisymmetric resonances	First	341.52	17	32	13	20
	Third	927.2	39	59	28	37
Structural resonances	Breathing	420.85	20	38	16	26
	Ovalling	933.36	40	68	28	37

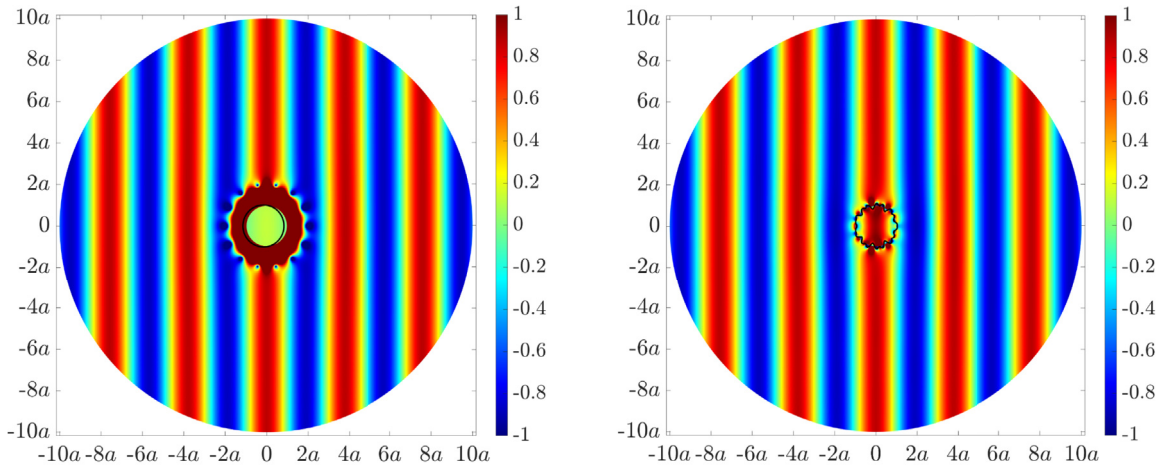

(a)

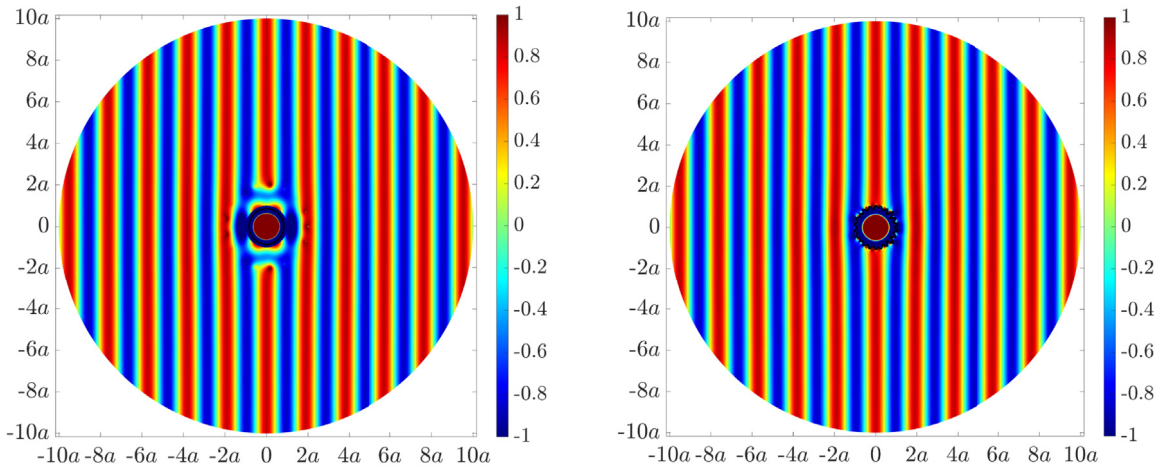

(b)

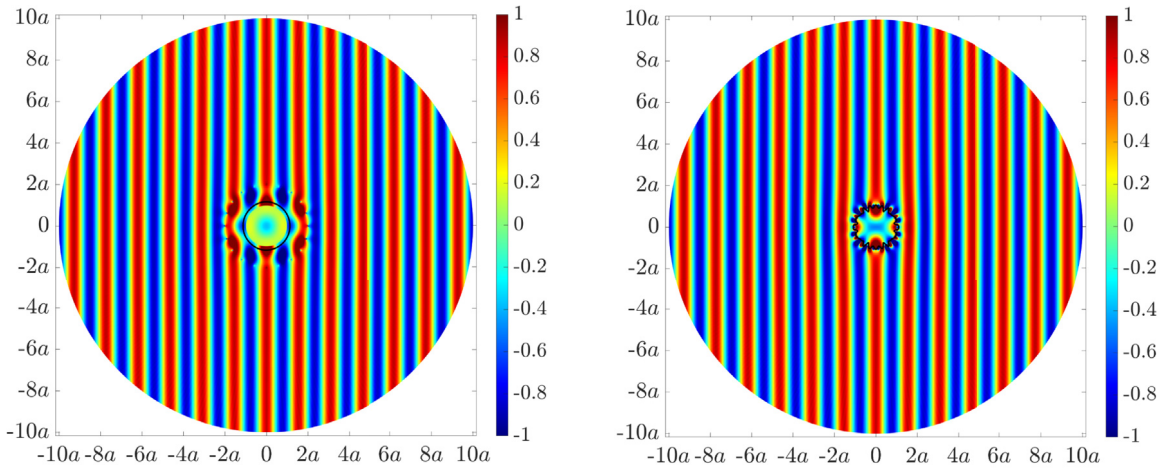

(c)

Fig. 7. ANCL (left) and ASACL (right) at $M = 0.12$ for the (a) first acoustic spinning resonance, (b) first acoustic axisymmetric resonance, (c) first structural resonance.

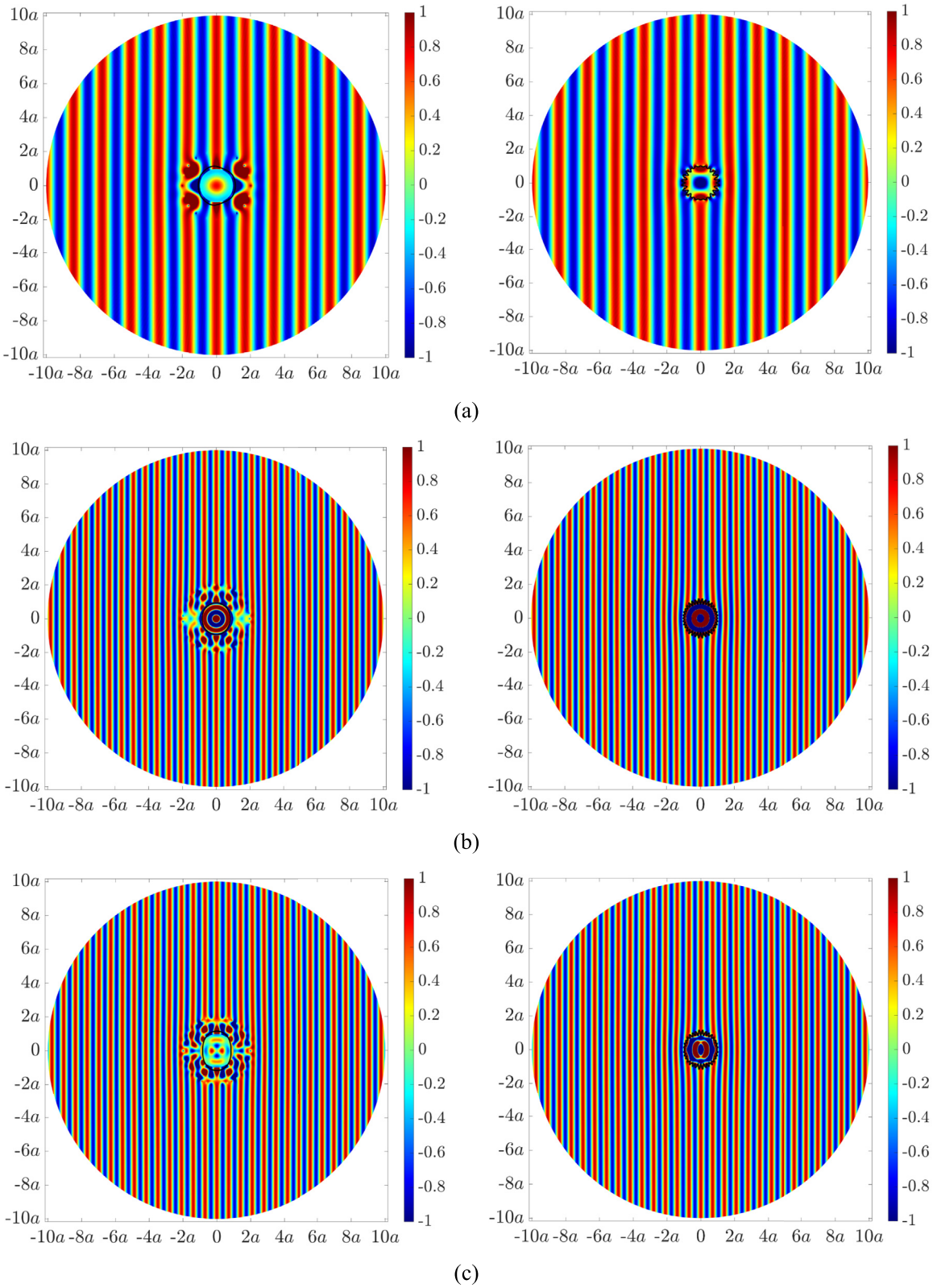

Fig. 8. ANCL (left) and ASACL (right) at $M = 0.12$ for the (a) third acoustic spinning resonance, (b) third acoustic axisymmetric resonance, (c) third structural resonance.

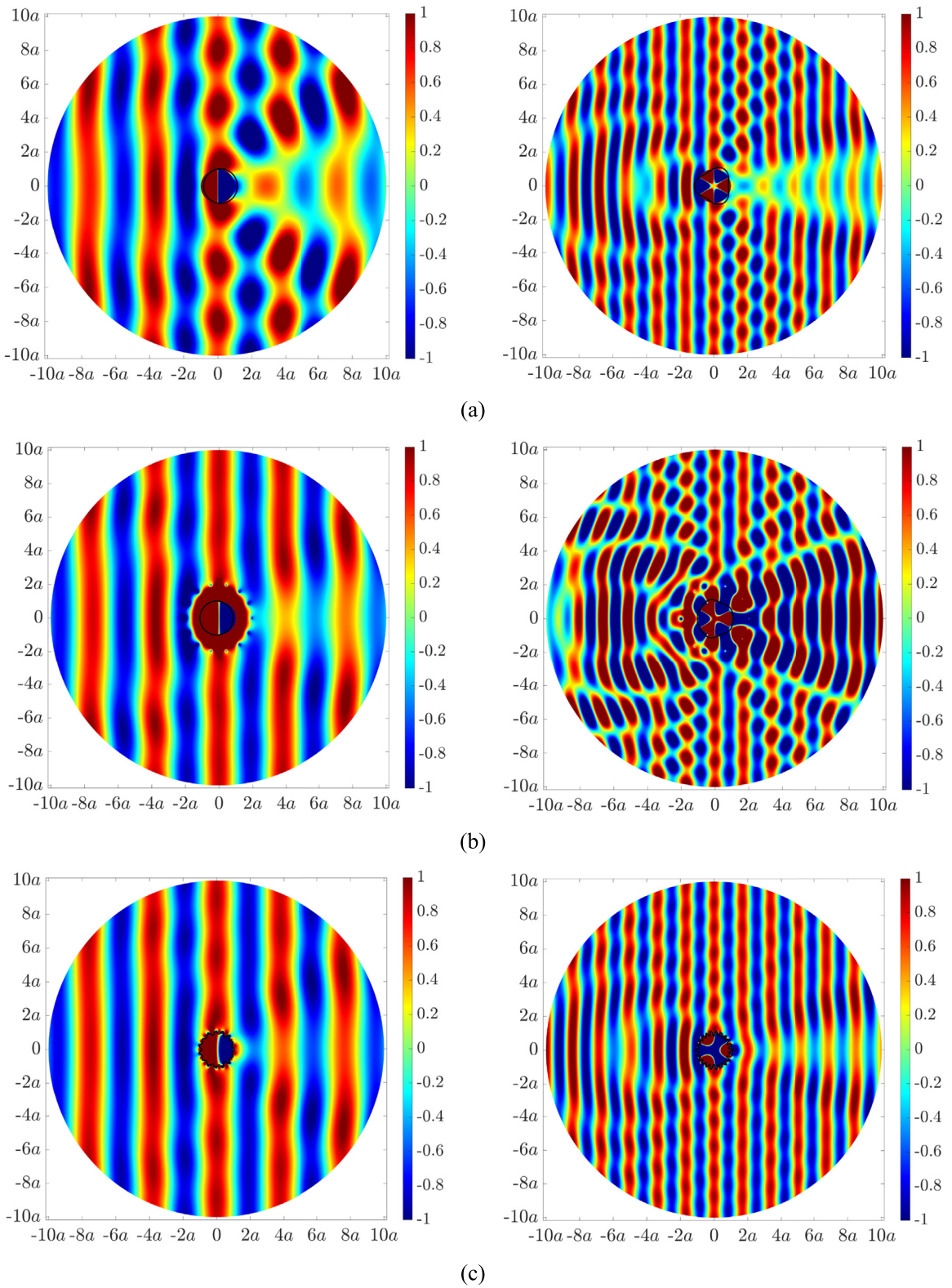

Fig. 9. (a) Acoustic pressure fields (in Pascal) at $M = 0.12$ due to excitation of a cylindrical shell from an incident plane wave. Cloaked field in which the effects of flow are neglected during the cloaking process for (b) ANCL and (c) ASACL. Frequencies correspond to the first (left) and third (right) acoustic spinning resonances.

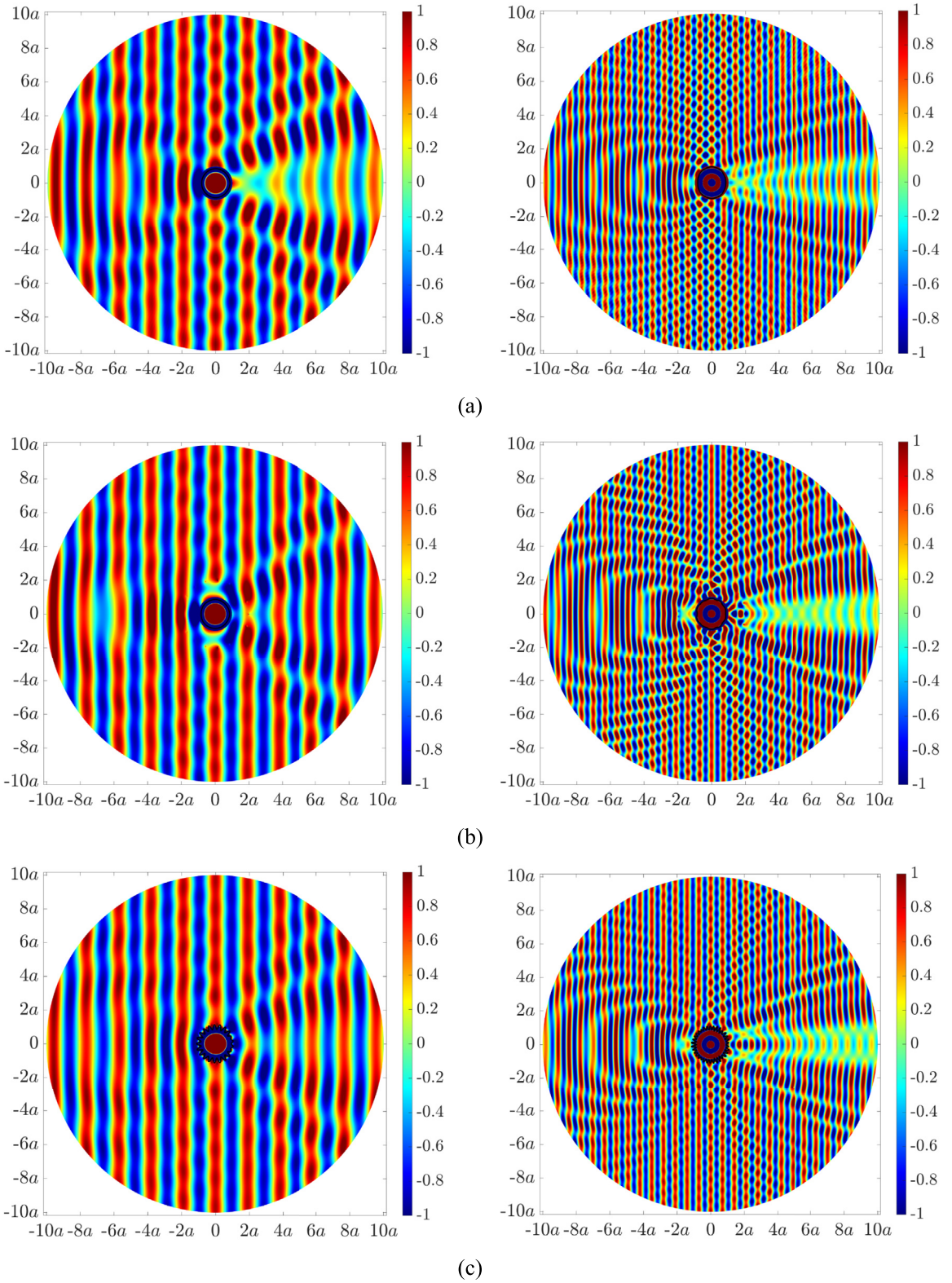

Fig. 10. (a) Acoustic pressure fields (in Pascal) at $M = 0.12$ due to excitation of a cylindrical shell from an incident plane wave. Cloaked field in which the effects of flow are neglected during the cloaking process for (b) ANCL and (c) ASACL. Frequencies correspond to the first (left) and third (right) acoustic axisymmetric resonances.

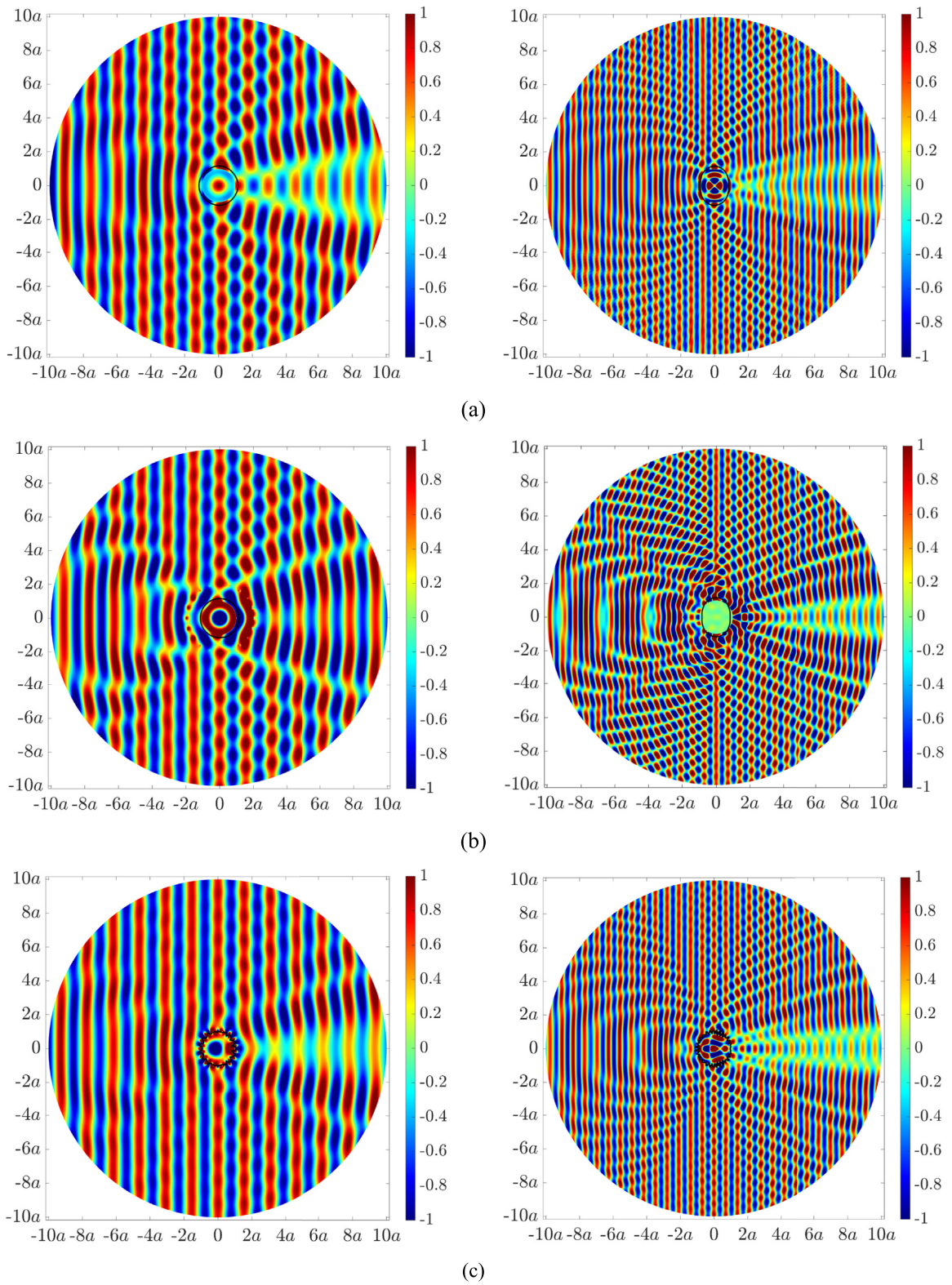

Fig. 11. (a) Acoustic pressure fields (in Pascal) at $M = 0.12$ due to excitation of a cylindrical shell from an incident plane wave. Cloaked field in which the effects of flow are neglected during the cloaking process for (b) ANCL and (c) ASACL. Frequencies correspond to the first (left) and third (right) structural resonances.

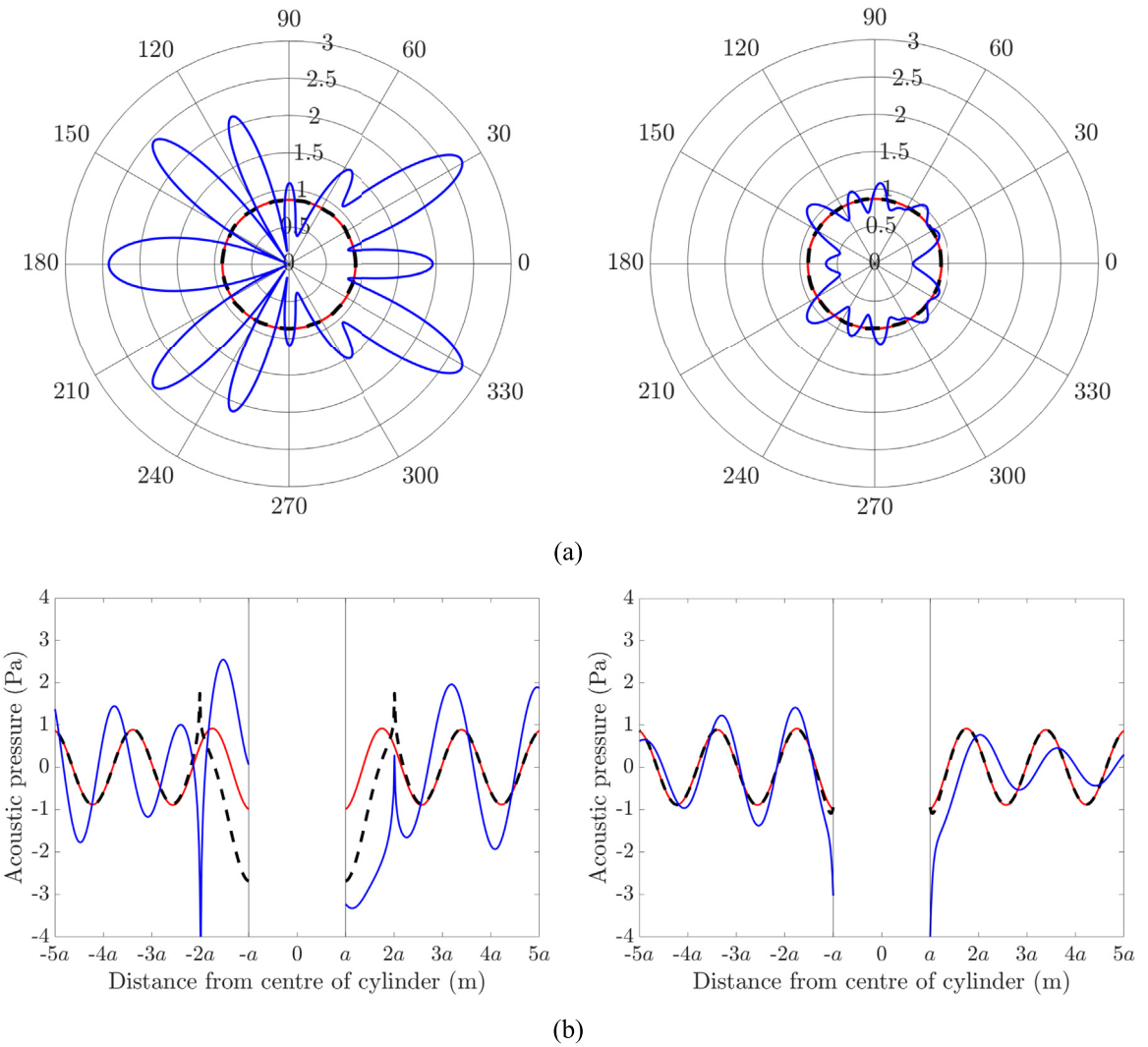

Fig. 12. (a) Acoustic directivities at a radial distance of $r = 3a$ and (b) acoustic pressure as a function of distance from the elastic shell along $\theta = 0$ corresponding to the incident acoustic field (solid red line), actively cloaked pressure accounting for flow of $M = 0.12$ (dashed black line) and actively cloaked pressure without accounting for flow (solid blue line), using ANCL (left) and ASACL (right) at the third acoustic spinning resonance of the cylindrical shell under incident plane wave excitation. (For interpretation of the references to colour in this figure legend, the reader is referred to the Web version of this article.)

axisymmetric resonance (Fig. 7(b)) and the structural breathing resonance (Fig. 7(c)). Using ANCL, the resultant controlled field resembles that of the convected incident field beyond the control source perimeter. Using ASACL, the cloaked field immediately takes effect beyond the control force perimeter corresponding to the surface of the shell. Similar results to Fig. 7 are included in Fig. 8 for the third acoustic and structural resonances, whereby a cloaked acoustic field beyond the circumferential array of control sources is achieved using ANCL, whereas the entire exterior acoustic field beyond the surface of the shell is cloaked using ASACL.

The acoustic performance of the cloaking process when the convected flow field is not accounted for is shown in Figs. 9–11 at both the first and third acoustic and structural resonances. Figs. 9(a)-11(a) present the uncontrolled acoustic pressure for a plane wave impinging on the elastic cylindrical shell (also known as the primary acoustic field). Figs. 9(b)-11(b) present the resultant field when cloaking is attempted using ANCL neglecting convective effects. Figs. 9(c)-11(c) present the resultant field when cloaking is attempted using ASACL neglecting convective effects. Comparison of Figs. 9(b)-11(b) with Figs. 9(c)-11(c) reveals that when using ANCL, any departure in the cloaking process yields significantly greater deviation of the resultant field from that of the desired field compared to using ASACL.

An error analysis of the active cloaking results is presented by examining the acoustic directivity, corresponding to the absolute acoustic pressure evaluated at a specific radial distance for all field points along the circumference, as well as the real acoustic pressure as a function of distance from the cylinder centre. Figs. 12(a)–14(a) present the acoustic directivity at $r = 3a$ for the incident field, the actively cloaked field when accounting for flow, and the controlled field when neglecting flow, using

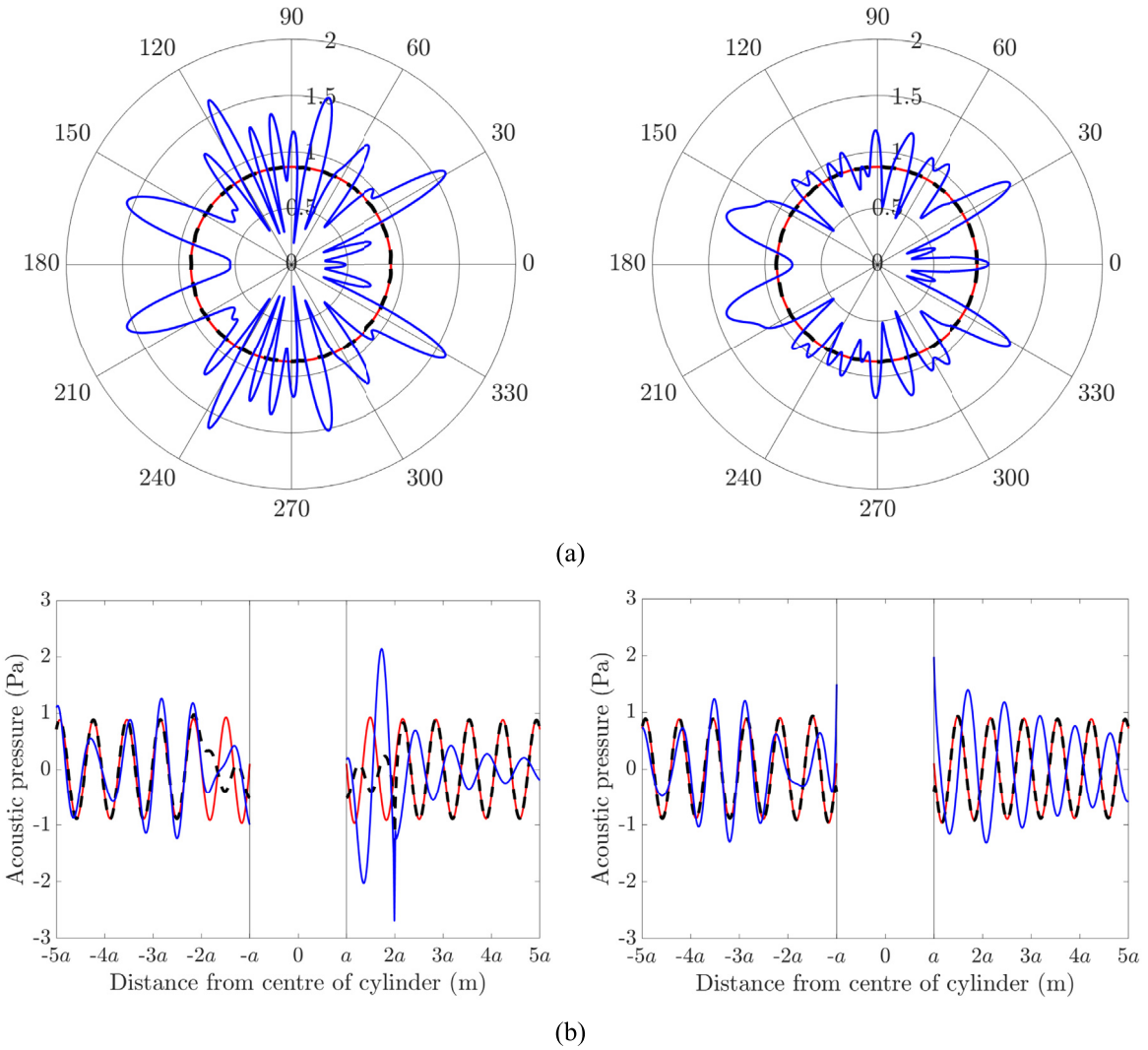

Fig. 13. (a) Acoustic directivities at a radial distance of $r = 3a$ and (b) acoustic pressure as a function of distance from the elastic shell along $\theta = 0$ corresponding to the incident acoustic field (solid red line), actively cloaked pressure accounting for flow of $M = 0.12$ (dashed black line) and actively cloaked pressure without accounting for flow (solid blue line), using ANCL (left) and ASACL (right) at the third acoustic axisymmetric resonance of the cylindrical shell under incident plane wave excitation. (For interpretation of the references to colour in this figure legend, the reader is referred to the Web version of this article.)

ANCL (left column) and ASACL (right column). Both control strategies exhibit identical directivities of the cloaked and incident fields when accounting for convection, but the resultant directivity significantly deviates from that of the incident field when neglecting convection. This effect is more pronounced using ANCL than using ASACL. This is attributed to the fact that since ASACL employs mechanical excitation, the Doppler effect is only applied to the radiated acoustic field. However, for ANCL which employs acoustic excitation, the Doppler effect is enhanced due to the additional contributions from the incident component of the acoustic control sources as well as the scattered and radiated response. In Figs. 12(b)-14(b), the same results are compared as a function of distance from the cylinder centre along $\theta = 0$. Effective cloaking is observed from the control source perimeter of $2a$ for ANCL (left column), and from the shell surface for ASACL (right column). Significantly greater deviation of the resultant field from that of the desired field is observed using ANCL compared with ASACL, when the effect of flow is not taken into consideration.

5. Conclusions

Acoustic cloaking of an elastic structure in a moving fluid using active control methods has been presented. The vibro-acoustic responses of an elastic cylindrical shell in potential flow under plane wave, monopole source and radial point force excitation were derived using Taylor's transformations and Donnell-Mushtari shell theory. The shell equations of motion

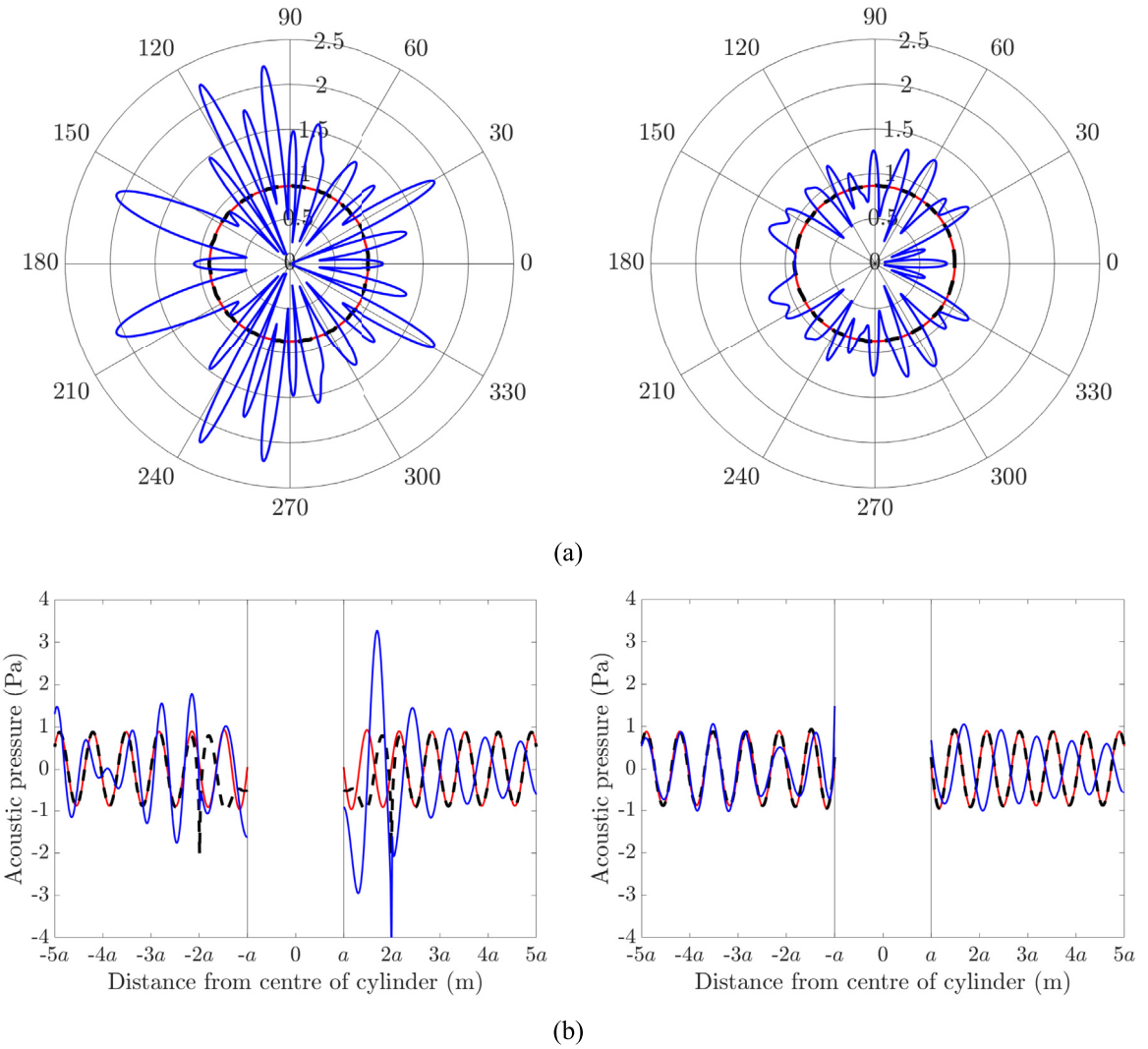

Fig. 14. (a) Acoustic directivities at a radial distance of $r = 3a$ and (b) acoustic pressure as a function of distance from the elastic shell along $\theta = 0$ corresponding to the incident acoustic field (solid red line), actively cloaked pressure accounting for flow of $M = 0.12$ (dashed black line) and actively cloaked pressure without accounting for flow (solid blue line), using ANCL (left) and ASACL (right) at the third structural resonance of the cylindrical shell under incident plane wave excitation. (For interpretation of the references to colour in this figure legend, the reader is referred to the Web version of this article.)

and boundary conditions on the interior and exterior shell surfaces were solved in the transformed domain. Scattering theory was applied to resolve the exterior and interior acoustic field coefficients for the different acoustic and structural excitation cases. Results for the first three acoustic spinning resonances, acoustic axisymmetric resonances and structural resonances were presented in the absence and presence of convected flow. Two active control approaches were implemented to acoustically cloak the elastic cylindrical shell in a moving fluid. In the first control approach using ANCL, acoustic control sources in the exterior fluid domain were uniformly distributed in a circumferential array around the cylindrical shell. In the second control approach using ASACL, point control forces were uniformly distributed to directly excite the elastic shell. ASACL was shown to have several distinct advantages over ANCL. First, the control effort was reduced as the number of required control inputs was lower. Second, using ASACL the cloaked exterior field took effect from the shell surface whereas using ANCL, the acoustic domain between the shell and acoustic control sources was uncloaked. Further, using ANCL, any departure in the cloaking process yielded significantly greater deviation of the resultant field from that of the desired field compared to using ASACL.

Declaration of competing interest

The authors declare that they have no known competing financial interests or personal relationships that could have appeared to influence the work reported in this paper.

Acknowledgements

The authors would like to acknowledge Winthrop Professor Jie Pan of The University of Western Australia for coining the phrase Active Structural Acoustic Cloaking.

References

[1] S.A. Cummer, D. Schurig, One path to acoustic cloaking, New J. Phys. 9 (2007) 45.
[2] A.N. Norris, Acoustic cloaking theory, Proc. Royal Soc. A 464 (2008) 2411–2434.
[3] Y. Cheng, F. Yang, J.Y. Xu, X.J. Liu, A multilayer structured acoustic cloak with homogeneous isotropic materials, Appl. Phys. Lett. 92 (2008) 151913.
[4] D. Torrent, J. Sánchez-Dehesa, Acoustic cloaking in two dimensions: a feasible approach, New J. Phys. 10 (2008), 063015.
[5] B.I. Popa, L. Zigoneanu, S.A. Cummer, Experimental acoustic ground cloak in air, Phys. Rev. Lett. 106 (2011) 253901.
[6] L. Zigoneanu, B.I. Popa, S.A. Cummer, Three-dimensional broadband omnidirectional acoustic ground cloak, Nat. Mater. 13 (2014) 352.
[7] Y.I. Bobrovnitskii, Impedance acoustic cloaking, New J. Phys. 12 (2010), 043049.
[8] M.D. Guild, A. Alu, M.R. Haberman, Cancellation of acoustic scattering from an elastic sphere, J. Acoust. Soc. Am. 129 (2011) 1355–1365.
[9] A.N. Norris, F.A. Amirkulova, W.J. Parnell, Source amplitudes for active exterior cloaking, Inverse Probl. 28 (2012) 105002.
[10] F. Guevara Vasquez, G.W. Milton, D. Onofrei, Active exterior cloaking for the 2D Laplace and Helmholtz equations, Phys. Rev. Lett. 103 (2009), 073901.
[11] F. Guevara Vasquez, G.W. Milton, D. Onofrei, Exterior cloaking with active sources in two dimensional acoustics, Wave Motion 48 (2011) 515–524.
[12] F. Guevara Vasquez, G.W. Milton, D. Onofrei, P. Seppecher, Transformation elastodynamics and active exterior acoustic cloaking. Acoustic Metamaterials, Springer, 2013, pp. 289–318.
[13] Y.I. Bobrovnitskii, A new solution to the problem of an acoustically transparent body, Acoust Phys. 50 (2004) 647–650.
[14] M. Rajabi, A. Mojahed, Active acoustic cloaking spherical shells, Acta Acust. united Ac. 104 (2018) 5–12.
[15] C. Scandrett, Scattering and active acoustic control from a submerged spherical shell, J. Acoust. Soc. Am. 111 (2002) 893–907.
[16] C. Scandrett, Y. Shin, K. Hung, M. Khan, C. Lilian, Cancellation techniques in underwater scattering of acoustic signals, J. Sound Vib. 272 (2004) 513–537.
[17] J. Cheer, Active control of scattered acoustic fields: cancellation, reproduction and cloaking, J. Acoust. Soc. Am. 140 (2016) 1502–1512.
[18] D. Eggler, H. Chung, F. Montiel, J. Pan, N. Kessissoglou, Active noise cloaking of 2D cylindrical shells, Wave Motion 87 (2019) 106–122.
[19] E. Friot, C. Bordier, Real-time active suppression of scattered acoustic radiation, J. Sound Vib. 278 (2004) 563–580.
[20] E. Friot, R. Guillermin, M. Winninger, Active control of scattered acoustic radiation: a real-time implementation for a three-dimensional object, Acta Acust. united Ac. 92 (2006) 278–288.
[21] C. García-Meca, S. Carloni, C. Barceló, G. Jannes, J. Sánchez-Dehesa, A. Martínez, Analogue transformations in physics and their application to acoustics, Sci. Rep. 3 (2013) 2009.
[22] H. Ryoo, W. Jeon, Effect of compressibility and non-uniformity in flow on the scattering pattern of acoustic cloak, Sci. Rep. 7 (2017) 2125.
[23] X. Huang, S. Zhong, O. Stalnov, Analysis of scattering from an acoustic cloak in a moving fluid, J. Acoust. Soc. Am. 135 (2014) 2571–2580.
[24] U. Iemma, G. Palma, Convective correction of metafluid devices based on Taylor transformation, J. Sound Vib. 443 (2019) 238–252.
[25] X. Huang, S. Zhong, X. Liu, Acoustic invisibility in turbulent fluids by optimised cloaking, J. Fluid Mech. 749 (2014) 460–477.
[26] Y. He, S. Zhong, X. Huang, Extensions to the acoustic scattering analysis for cloaks in non-uniform mean flows, J. Acoust. Soc. Am. 146 (2019) 41–49.
[27] D. Eggler, M. Karimi, N. Kessissoglou, Active acoustic cloaking in a convected flow field, J. Acoust. Soc. Am. 146 (2019) 586–594.
[28] M. Païdoussis, S. Price, S.-Y. Ang, Ovalling oscillations of cylindrical shells in cross-flow: a review and some new results, J. Fluid Struct. 2 (1988) 95–112.
[29] N. Peake, On the behaviour of a fluid-loaded cylindrical shell with mean flow, J. Fluid Mech. 338 (1997) 387–410.
[30] M. Amabili, R. Garziera, Vibrations of circular cylindrical shells with nonuniform constraints, elastic bed and added mass. Part II: shells containing or immersed in axial flow, J. Fluid Struct. 16 (2002) 31–51.
[31] K. Taylor, Acoustic generation by vibrating bodies in homentropic potential flow at low Mach number, J. Sound Vib. 65 (1979) 125–136.
[32] A.W. Leissa, Vibration of Shells, American Institute of Physics, New York, 1993.
[33] M.C. Junger, D. Feit, Sound, Structures, and Their Interaction, MIT Press, Cambridge, MA, 1986.
[34] P.A. Martin, Multiple Scattering: Interaction of Time-Harmonic Waves with N Obstacles, Cambridge University Press, 2006.
[35] A. Agarwal, A.P. Dowling, Low-frequency acoustic shielding by the silent aircraft airframe, AIAA J. 45 (2007) 358–365.
[36] M.S. Howe, Acoustics of Fluid-Structure Interactions, Cambridge university press, 1998.
[37] K. Taylor, A transformation of the acoustic equation with implications for wind-tunnel and low-speed flight tests, Proc. Royal Soc. A 363 (1978) 271–281.
[38] M. Karimi, P. Croaker, N. Peake, N. Kessissoglou, Acoustic scattering for rotational and translational symmetric structures in nonuniform potential flow, AIAA J. (2017) 3318–3327.
[39] R.D. Blevins, Flow-induced Vibration, Van Nostrand Reinhold Company, New York, 1977.
[40] A. Rona, The acoustic resonance of rectangular and cylindrical cavities, J. Algorithms Comput. Technol. 1 (2007) 329–356.
[41] H. Peters, N. Kessissoglou, S. Marburg, Modal decomposition of exterior acoustic-structure interaction problems with model order reduction, J. Acoust. Soc. Am. 135 (2014) 2706–2717.
[42] B. Widrow, S.D. Stearns, Adaptive Signal Processing, Prentice-Hall, Englewood Cliffs, NJ, 1985.
[43] N. Han, S. Feng, X. Qiu, Active control of one-dimension impulsive reflection based on a prediction method, J. Acoust. Soc. Am. 127 (2010) 1193–1196.
[44] N. Han, X. Qiu, S. Feng, Active control of three-dimension impulsive scattered radiation based on a prediction method, Mech. Syst. Signal Process. 30 (2012) 267–273.